Spin Coating of Colloidal Suspensions

Timothy J. Rehg and Brian G. Higgins
Dept. of Chemical Engineering, University of California, Davis, CA 95616

The coupled, unsteady Navier-Stokes, convective diffusion, and thermal energy equations that describe spin coating of colloidal suspensions are solved numerically. The theoretical model, absent of any adjustable parameters, is used to explore the effects of angular velocity, initial solvent weight fraction, solvent properties and spin coating protocol on the evolution of temperature and concentration profiles in the liquid film during spin coating. The predicted coated film thickness is found to be in excellent quantitative agreement with spin coating experiments performed with both hard-sphere and nonhard-sphere suspensions of monodisperse latex particles in water. The coated film thickness, determined by ellipsometry, is shown to depend on the inverse square root of the angular velocity except at high ionic strength when the dependence on angular velocity is weaker. Timescales that characterize spin coating of colloidal suspensions are shown to be quite different from those that characterize spin coating of polymer solutions, and consequently simple models for predicting the coated film thickness of polymer solutions (Bornside et al., 1991; Lawrence, 1989) are shown to be inadequate for colloidal suspensions. Rapid substrate acceleration, high rotation rates, partial saturation of the overlying gas phase, and high initial solids concentration are identified as spin coating protocols that suppress a convective instability that produces radial striations in the coated film.

Introduction

Optical coatings prepared from colloidal suspensions have proven to be superior to traditional vacuum deposition coatings in the optics of high-power laser systems, because they exhibit high damage thresholds, are relatively easy to deposit, and are less expensive to fabricate. In addition, colloidal coatings are advantageous, because the refractive index of the coated film can be tailored to a specific application by manipulating the colloidal forces that dictate film porosity. Dip coating and spin coating are the principal means by which colloidal coatings have been applied to laser optics.

Spin coating is the preferred method when many layers need to be sequentially deposited. For example, Thomas (1989) has shown that high reflecting mirrors with 99% reflection of the incident beam can be fabricated by spin-coating a multilayer quarterwave stack consisting of 18 layer pairs of high/low refractive index materials. In a typical spin coating operation, an excess of the colloidal suspension is dispensed on a stationary (or slowly rotating) substrate that is subsequently accelerated to a preset rotation rate. Through the action of centrifugal force, most of the suspension is initially flung off the substrate leaving behind a film that continues to thin by radial outflow and solvent evaporation. As the suspension becomes more concentrated, its viscosity rises and then eventually becomes so large that radial outflow effectively ceases. The film continues to thin, however, until the solvent has evaporated thoroughly and a "dry" film of the suspended material is left.

Because spin coating offers a means whereby thin, uniform films of precise thickness can be reproducibly coated, it has found widespread use in a variety of manufacturing processes. Much of the recent theoretical effort in spin coating has been directed at applications involving polymer solutions for microlithography (Bornside et al., 1989, 1991; Lawrence, 1988, 1990; Ohara et al., 1989; Meyerhofer, 1978) and has for the most part, been based on low Reynolds number hydrodynamics. These efforts have resulted in two simple theories that relate coated film thickness to physical properties of the coating solution and spin speed of the disk.

The first, developed by Meyerhofer (1978) and later modified by Bornside et al. (1991), assumes that (i) convective thinning due to radial outflow is not affected by solvent evaporation, and (ii) the coated film thickness is determined when the con-

vective thinning rate (due to radial outflow) is equal to the solvent evaporation rate. The expression they derive for the coated film thickness h_f is:

$$h_f=(1-\omega_o)\left[\left(\frac{3\nu_o}{2\Omega_o^2}\right)\left(\frac{P_s^{\text{vap}}M_s}{RT_o}\right)k_m(\omega_o-\omega_\infty)\right]^{1/3} \tag{1a}$$

where ω_o is the initial weight fraction of solvent, ν_o is the initial kinematic viscosity of the coating solution, Ω_o is the spin speed of the disk, and k_m is the mass-transfer coefficient taken to be proportional to $\Omega_o^{1/2}$. (For other symbols, see the Notation section).

The second theory, developed by Lawrence (1988, 1990), is based on the assumption that thinning due to radial outflow ceases when the concentration boundary layer spans the thinning film and is given by:

$$h_f=C(1-\omega_o)(\nu_o\mathfrak{D}_o)^{1/4}\Omega_o^{-1/2} \tag{1b}$$

where C is an adjustable parameter of order $O(1)$ and $\mathfrak{D}_o$ is the initial diffusivity. Both models predict that the coated film thickness is proportional to $\Omega_o^{-1/2}$, a result often observed in experimental investigations of spin coating (Meyerhofer, 1978; Lai, 1979; Daughton and Givens, 1982; Chen, 1983; Bornside et al., 1991). We are unaware of similar studies directed toward colloidal systems, though one can suppose (perhaps naively) that these models should also apply to colloidal systems. This turns out not to be the case.

In this article, we develop a mathematical model that describes spin coating of colloidal suspensions based on the self-similar form of the Navier-Stokes, convective diffusion, and thermal energy equations. Inertial effects, important during spin-up, are included. Our aim is to develop a theory for spin-coating colloidal suspensions that is predictive and useful for evaluating disk spin-up protocols for coating large area optics.

The importance of disk spin-up protocols has been addressed by Frasch and Saremski (1982) for coating polymer solutions. They showed that slow substrate acceleration rates during spin-up are more likely to result in coated films that exhibit radial striations. We and others have also observed the same instability in spin coating of colloidal suspensions. The colloidal particles are typically in the 20–30 nm range; depending on the optical application, the coating thickness is in the range of 20–100 nm. Films this thin are achieved by spin-coating low-viscosity suspensions (10^{-3} Pa·s) at moderate to high rotation rates (2,000–6,000 rpm). One can readily show from simple order of magnitude arguments that during spin-up inertial effects are significant in these coating systems and cannot be ignored when studying the dynamics of film thinning.

We describe the mathematical problem and the constitutive models used for the suspension viscosity and diffusivity, and then discuss the finite difference formulation and the numerical algorithm employed to solve the nonlinear algebraic equation set to which the nonlinear partial differential equations reduce. Subsequently, we describe our experimental system, spin coating procedures, and film thickness measurements. The model is validated by our experimental results with hard-sphere and nonhard-sphere suspensions of monodispersed latex particles in water and by measurements of the coated film thickness that agree well with the computed values. Also discussed are transport processes that determine the dynamics of film thinning and why Eqs. 1a and 1b are inadequate for predicting the coated film thickness in our system. Knowledge of the dynamics of film thinning is used to study different spinning protocols useful for suppressing the convective instability that produces radial striations in the coated film, the mechanism of which was addressed previously (Rehg and Higgins, 1992). Finally, we summarize our results, draw some conclusions, and discuss how colloidal forces might affect coating microstructure.

Mathematical Formulation

For a planar interface, the Navier-Stokes, convective diffusion, and thermal energy equations can be reduced to a time-dependent, one-dimensional boundary value problem by taking the velocity, $\boldsymbol{u}$, solvent weight fraction, ω, temperature, T, and film thickness, h, to be of the form:

$$\boldsymbol{u}=rf(z,t)\boldsymbol{e}_r+rg(z,t)\boldsymbol{e}_\theta+w(z,t)\boldsymbol{e}_z, \tag{2a}$$

$$\omega=\omega(z,t),\ T=T(z,t),\ h=h(t), \tag{2b-d}$$

where $\boldsymbol{e}_r$, $\boldsymbol{e}_\theta$, and $\boldsymbol{e}_z$ are the base vectors for a cylindrical coordinate system. When Eq. 2 is substituted into the Navier-Stokes, convective diffusion and thermal energy equations, the following equation set, in dimensionless form, is obtained:

$$2F+W_\eta=0 \tag{3a}$$

$$F_\tau+F^2+WF_\eta=\frac{1}{Re}(\bar{\nu}(\omega,\Theta)F_\eta)_\eta+G^2 \tag{3b}$$

$$G_\tau+2FG+WG_\eta=\frac{1}{Re}(\bar{\nu}(\omega,\Theta)G_\eta)_\eta \tag{3c}$$

$$\omega_\tau+W\omega_\eta=\frac{1}{ReSc}(\bar{\mathfrak{D}}(\omega,\Theta)\omega_\eta)_\eta \tag{3d}$$

$$\Theta_\tau+W\Theta_\eta=\frac{1}{RePr}\Theta_{\eta\eta}. \tag{3e}$$

The variables are made dimensionless according to:

$$\eta=\frac{z}{h_o},\quad \tau=t\Omega_o,$$

$$F=\frac{f}{\Omega_o},\ G=\frac{g}{\Omega_o},\ W=\frac{w}{h_o\Omega_o},$$

$$\Theta=\frac{T}{T_o},\ H=\frac{h}{h_o}. \tag{4}$$

The unit of time is Ω_o^{-1}, where Ω_o is the final angular velocity of the disk. The unit of length is h_o, the initial film thickness. Temperature is scaled with the substrate temperature T_o and the solvent weight fraction is left unscaled. Note that $\bar{\nu}$ and $\bar{\mathfrak{D}}$ are the dimensionless kinematic viscosity and mass diffusivity made dimensionless with their initial values ν_o and $\mathfrak{D}_o$, respectively. The thermal diffusivity is taken to be constant in

this analysis and, therefore, does not appear explicitly in Eq. 3e. The dimensionless groups that accompany this set of equations are the Reynolds, Schmidt and Prandtl numbers defined as:

$$Re=\frac{h_o^2\Omega_o}{\nu_o},\ Sc=\frac{\nu_o}{\mathfrak{D}_o},\ Pr=\frac{\nu_o}{\alpha_o}. \tag{5}$$

Bornside et al. (1989), Lawrence (1988, 1990), and Meyerhofer (1978) followed the early work of Emslie et al. (1958) and took inertial effects other than centrifugal to be negligible. As a result, their models (equivalent to neglecting the lefthand side of Eqs. 3b-3c are unable to describe the dynamics of spin-up when inertial effects are important (Higgins, 1986; Rehg and Higgins, 1988). Recently, Ohara et al. (1989) proposed Eqs. 2-5 as a model of spin coating, but they did not consider inertial effects as these effects were apparently unimportant in their study. In this article, we follow Ohara et al.'s development and consider short time events where inertia is important, for example, substrate acceleration protocols and growth of instabilities.

At the disk surface we specify no slip, no penetration, and constant temperature:

$$F(0,\tau)=W(0,\tau)=\omega_\eta(0,\tau)=0,\ G(0,\tau)=\frac{\Omega(\tau)}{\Omega_o},\ \Theta(0,\tau)=1. \tag{6}$$

The inertia of the spin coater is accounted for by specifying the acceleration ramp $\Omega(\tau)$. For our calculations, the acceleration rate is taken to be constant.

Rehg and Higgins (1988) have shown that the overlying gas phase exerts negligible shear on the liquid film. Therefore, the traction condition that is satisfied at the free surface, $\eta=H(\tau)$, is:

$$F_\eta=G_\eta=0. \tag{7a}$$

Continuity of mass and heat flux require the following conditions be satisfied at the free surface:

$$\frac{\overline{\mathfrak{D}}(\omega,\Theta)}{1-\omega}\frac{\partial\omega}{\partial\eta}=-Bi\frac{\bar\rho}{\rho}(\bar\omega-\omega_\infty), \tag{7b}$$

$$\frac{\partial\Theta}{\partial\eta}=-N\frac{Pr}{Sc}Bi\frac{\bar\rho}{\rho}(\bar\omega-\omega_\infty)-Bi_h(\Theta-\Theta_\infty), \tag{7c}$$

where $\bar\omega$ is the mass fraction of solvent in the gas phase in equilibrium with the liquid film, $\bar\rho/\rho$ is the ratio of the gas-phase and liquid-phase densities, and Θ_∞ is the temperature in the gas phase far from the film. The dimensionless groups Bi and Bi_h are the Biot numbers for mass and heat transfer, and N is a dimensionless enthalpy of vaporization, each defined by:

$$Bi=\frac{k_m h_o}{\mathfrak{D}_o},\ Bi_h=\frac{k_h h_o}{k_o},\ N=\frac{\Delta H_{vap}}{T_o C_p}. \tag{8}$$

where C_p is the constant pressure heat capacity, and k_m and k_h are the mass- and heat-transfer coefficients for flow over a rotating disk given by the relations (Sparrow and Gregg, 1959; Krieth et al., 1959):

$$k_m=f(Sc_g)\left(\frac{\Omega_i}{\nu_g}\right)^{0.5}\mathfrak{D}_g \tag{9}$$

$$k_h=f(Pr_g)\left(\frac{\Omega_i}{\nu_g}\right)^{0.5}k_g. \tag{10}$$

The function f is determined once the gas-phase Prandtl (Pr_g) and Schmidt (Sc_g) numbers are specified; ν_g is the gas-phase kinematic viscosity, Ω_i is the angular velocity of the free surface (time-dependent), $\mathfrak{D}_g$ is the solvent diffusivity in the overlying gas phase, and k_g is the thermal conductivity of the gas phase. Ramping the substrate to its final angular velocity and film spin-up are both expected to influence the gas-phase transport environment. These effects are qualitatively accounted for by taking the mass- and heat-transfer coefficients to depend on Ω_i. That is, the motion in the overlying gas phase is approximated as a quasi-steady flow over a rotating disk since the time scale for spin-up of a fluid over a rotating surface is smaller than that for film thinning (Benton, 1966; Homsy and Hudson, 1968; Ohara et al., 1989; Rehg and Higgins, 1988).

To use Eqs. 9-10 the function f must be determined. Krieth et al. (1959) and Sparrow and Gregg (1959) report limited numerical data for the mass- and heat-transfer coefficients as a function of the Schmidt and Prandtl numbers. For $0.74\le$ (Pr_g or Sc_g) ≤ 10, the data is reasonably well represented by the following correlation:

$$f(Pr_g \text{ or } Sc_g)=0.389\ (Pr_g \text{ or } Sc_g)^{0.457}. \tag{11}$$

However, to compare our model with our experiments, it was necessary in some cases to extrapolate Eq. 11 to $Sc_g=0.59$. We estimate the error in this extrapolation to be less than 5%.

Continuity of mass requires that the following kinematic condition hold at the free surface:

$$\frac{dH}{d\tau}=W-\frac{Bi}{ReSc}\frac{\bar\rho}{\rho}(\bar\omega-\omega_\infty). \tag{12}$$

The instantaneous convective thinning rate is simply the axial velocity evaluated at the film surface, $W(\eta=H(\tau),\tau)$, which for convenience is denoted by $\dot C$. The instantaneous evaporative thinning rate corresponds to the second term on the righthand side of Eq. 12 and is denoted by $\dot E$. The cumulative convective and evaporative thinning losses at time τ are given by the following relations:

$$I\dot C=\int_{s=0}^{s=\tau}\dot C\,ds \tag{13a}$$

$$I\dot E=\int_{s=0}^{s=\tau}\dot E\,ds. \tag{13b}$$

These definitions prove useful, as will be discussed later.

As our initial conditions, we take the fluid to be stationary and the concentration and temperature profiles to be uniform:

Table 1. Solvent Material Properties

Water	Ethanol	Air
$\mu_s = \exp\left[1{,}515.677\left(\frac{1}{T}-\frac{1}{283.16}\right)-\ln(1{,}000)\right]$ Pa·s	$\log\mu_s = \left[686.64\left(\frac{1}{T}-\frac{1}{300.88}\right)-3\right]$ Pa·s	$\bar{\rho} = 1.185\left(\frac{298.15}{T}\right)$ kg/m^3
$\rho_s = 1{,}000$ kg/m^3	$\log\rho_s = 789$ kg/m^3	$\nu_g = 1.562\times10^{-5}$ m^2/s
$\nu_s = \exp\left[1{,}515.677\left(\frac{1}{T}-\frac{1}{283.16}\right)-2\ln(1{,}000)\right]$ m^2/s	$\nu_s = \left[686.64\left(\frac{1}{T}-\frac{1}{300.88}\right)-5.897\right]$ m^2/s	$k_g = 2.6397\times10^{-2}$ w/(m·K)
$k_s = 0.609$ W/(m·K)	$k_s = 0.1672$ W/(m·K)	$Pr_g = 0.74$
$C_p = 4{,}182.8$ J/(kg·K)	$C_p = 2{,}452.15$ J/(kg·K)	$\mathcal{D}_g$ (water in air) $= 2.63\times10^{-5}$ m^2/s
$\alpha_s = 1.1457\times10^{-7}$ m^2/s	$\alpha_s = 8.6394\times10^{-8}$ m^2/s	Sc_g (water in air) $= 0.5939$
$\Delta H_{vap} = 1.722$ J/kg	$\Delta H_{vap} = 1.613$ J/kg	$\mathcal{D}_g$ (ethanol in air) $= 1.27\times10^{-5}$ m^2/s
$P_s^{vap} = \exp\left[11.6703-\frac{3{,}816.44}{T-46.13}\right]$ atm	$P_s^{vap} = \exp\left[12.2786-\frac{3{,}803.98}{T-41.68}\right]$ atm	Sc_g (ethanol in air) $= 1.23$

$$F(\eta,0) = G(\eta,0) = W(\eta,0) = 0,$$

$$\Theta(\eta,0) = H(0) = 1,\ \omega(\eta,0) = \omega_o. \quad (14)$$

The equations derived thus far apply to a generic spin-coating system with a single solvent. To close the set of equations and make the model specific to colloidal systems, it is necessary to specify the constitutive relations for the viscosity and diffusivity. Several investigators (Russel et al., 1989; de Kruif et al., 1985, 1987) have shown that the viscosity of a hard-sphere colloidal suspension can be described by:

$$\mu = \mu_s\left(1-\frac{\phi}{\phi_m}\right)^{-2}, \quad (15)$$

where ϕ is the volume fraction of suspended material, μ_s is the solvent viscosity, and ϕ_m is the volume fraction when the suspension viscosity becomes unbounded. For simplicity, we ignore shear thinning effects and take $\phi_m = 0.63$ (cf. Russel et al., 1989). The importance of shear thinning in our experiments will be discussed later. Colloidal suspensions that do not behave as hard spheres often have the same viscosity relation except with a modified value of ϕ_m. For example, Buscall et al. (1982) were able to correlate their viscosity measurements for a colloidal suspension of charged latex spheres by setting $\phi_m = 0.15$ in Eq. 15.

Batchelor (1976) has derived the following relation for the diffusivity of hard-sphere colloidal suspensions:

$$\mathcal{D} = \tilde{\mathcal{D}}(1+1.45\phi) \quad (16)$$

where $\tilde{\mathcal{D}}$ is given by the Stokes-Einstein relation: $\tilde{\mathcal{D}} = k_b T/6\pi\mu_s a$. This particular form of the diffusivity has been shown in some cases to predict the diffusivity of colloidal particles up to a volume fraction of 0.3 (de Kruif et al., 1985). We will show that the thinning process is essentially complete at volume fractions well within the range of validity of Eq. 16, thereby justifying its use.

Because the latex spheres used in our experiments had a density of 1,055 kg/m^3, the density of the coating fluid was taken to be constant and equal to that of water. The thermal conductivity and thermal diffusivity of the coating fluid were taken to be constant and equal to those of water. Since the osmotic pressure of the colloidal suspension is negligible for systems such as those used here (de Kruif et al., 1987), the colloidal particles do not influence the solvent activity and the solvent vapor pressure is equal to its saturation vapor pressure. The gas-phase concentration of solvent in equilibrium with the coating solution is then given by $\bar{\omega} = (y_s\gamma)/(1-y_s(1-\gamma))$, where γ is the molecular weight ratio of solvent to air and $y_s = P_s^{vap}/P_{tot}$ is the gas-phase mole fraction of solvent at the free surface. The solvent properties used in the calculations are listed in Table 1.

The equations outlined above were solved with a fully implicit finite difference scheme. Because of the moving boundary, it was convenient to transform the time-dependent physical domain, $\eta\in[0,H(\tau)]$ to a fixed computational domain, $\xi\in[0,1]$. For large values of the Schmidt number, the prospect of sharp concentration gradients near the interface posed some difficulty with regard to how the finite difference grid was determined. The following transformation proved to be useful (Roberts, 1971):

$$\xi(\tau) = \frac{\ln\left[\dfrac{\beta+\dfrac{\eta}{H(\tau)}}{\beta-\dfrac{\eta}{H(\tau)}}\right]}{\ln\left[\dfrac{\beta+1}{\beta-1}\right]} \quad (17)$$

This transformation converts a variable grid spacing in the η-domain (physical domain $[0,H]$) to a uniform grid spacing in the ξ-domain (computational domain $[0,1]$). The parameter β controls the anisotropy in the grid spacing in the physical domain. Small values of β cluster grid points at the free surface, whereas large values of β tend to make the grid spacing uniform throughout the liquid film. To capture the velocity gradients at the disk and the concentration gradients at the free surface, 300 nodes with $\beta = 1.05$ were used in all cases. These values were taken from another study (Rehg and Higgins, 1992) based on a polymeric system where they were capable of resolving concentration gradients much steeper than those encountered in this study. The calculations were carried out on the CRAY Y-MP at the San Deigo Supercomputer Center.

A fully implicit finite difference scheme was used to solve

the nonlinear system of Eqs. 2—7 after they were transformed according to Eq. 17. All spatial derivatives were approximated by central difference, except in the continuity equation (Eq. 3a), where forward difference was used. Due to the nonlinear nature of the equation set, an iterative solution procedure was required. At time step m and iteration k, the $\underset{\sim}{G}_m^k$ field (a vector of unknowns of dimension N, where G is the azimuthal velocity and N is the number of spatial nodes) was determined by solving the finite difference form of Eq. 3c which can be expressed as:

$$\underset{\approx}{A} \cdot \underset{\sim}{G}_m^k = \underset{\sim}{D}. \tag{18}$$

To account for the explicit dependence of F, W, ω, Θ and H on G (the dependence on H occurs because the domain has been transformed, cf. Eq. 17, a successive substitution scheme was used; in this manner $\underset{\approx}{A}$ was determined from the values of F, W, ω, Θ and H at the $k-1$ iteration. $\underset{\approx}{A}$ and $\underset{\sim}{D}$ are given by:

$$\underset{\approx}{A} = \underset{\approx}{A}(\underset{\sim}{F}_m^{k-1}, \underset{\sim}{W}_m^{k-1}, \underset{\sim}{\omega}_m^{k-1}, \underset{\sim}{\Theta}_m^{k-1}, \underset{\sim}{H}_m^{k-1}) \tag{19a}$$

$$\underset{\sim}{D} = \underset{\sim}{D}(G_{m-1}) \tag{19b}$$

where G_{m-1} is the converged solution vector at the $m-1$ time step. At each iteration step, an identical procedure was used for the field variables ω and Θ. The procedure for the F-field is different only in that the nonlinear F^2 term in Eq. 2b was linearized by Newton's method rather than by successive substitution:

$$(F_m^k)^2 = 2F_m^k F_m^{k-1} - (F_m^{k-1})^2. \tag{20}$$

As a consequence, the finite difference form of Eq. 3b differs from Eq. 17 and is given by:

$$\underset{\approx}{B}(\underset{\sim}{F}_m^{k-1}, \underset{\sim}{W}_m^{k-1}, \underset{\sim}{\omega}_m^{k-1}, \underset{\sim}{\Theta}_m^{k-1}, \underset{\sim}{H}_m^{k-1}) \cdot \underset{\sim}{F}_m^k = \underset{\sim}{E}(\underset{\sim}{F}_m^{k-1}, \underset{\sim}{G}_m^{k-1}, \underset{\sim}{F}_{m-1}). \tag{21}$$

Because of the linearization and decoupling schemes described above, the linearized equation sets are tridiagonal and can be readily inverted with the Thomas algorithm to yield $\underset{\sim}{F}_m^k$, $\underset{\sim}{G}_m^k$, $\underset{\sim}{\omega}_m^k$, and $\underset{\sim}{\Theta}_m^k$.

The axial velocity field $\underset{\sim}{W}_m^k$ was determined from the finite difference form of the continuity equation Eq. 3a with $\underset{\sim}{F}_m^{k-1}$. The finite difference form was solved node by node due to the forward difference approximation of the derivative. The free surface value of $\underset{\sim}{W}_m^{k-1}$ was substituted into the finite difference form of Eq. 12 to yield $\underset{\sim}{H}_m^k$. The above algorithm was repeated until the relative error at each node, defined as:

$$\delta = \frac{|(\underset{\sim}{Q}_m^k)_i - (\underset{\sim}{Q}_m^{k-1})_i|}{|(\underset{\sim}{Q}_m^k)_i|} \tag{22}$$

was less than 10^{-6} for each of the dependent variables ($Q = F$, G, W, ω, Θ, H). This procedure was repeated at each time step until the volume fraction of solids at the free surface reached ϕ_m at which point the simulation was terminated. An alternative procedure was to terminate the simulation when the convective thinning rate became negligible compared to the evaporative thinning rate. Both procedures for terminating the simulation yielded the same mass of coating material deposited on the substrate.

Table 2. Sulfate Polystyrene Latex Properties (Lot No. 10-187-28)

Mean Diameter (nm):	19 ± 4
Density of Polystyrene (kg/m^3):	1055
Refractive Index of Polystyrene, n_d ($\lambda = 632.8$ nm) (Swalen et al., 1977):	1.5845
Surface Charge Density (C/m^2):	0.055

The model developed here does not address film shrinkage once convective thinning is negligible, and thus is is not capable of predicting film porosity or microstructure. Consequently, to compare theory with experiment, it was necessary to adjust the theoretical predicted film thickness to have a porosity equal to that of the experimentally measured film. The porosity of the coated film, ϵ, was determined indirectly by measuring the index of refraction of the film, n_p, by ellipsometry. The porosity of the coated film was then determined with the following relation (Yoldas, 1980):

$$\epsilon = \frac{n_p^2 - 1}{n_d^2 - 1} \tag{23}$$

where n_d is the index of refraction of the dense coating material.

Experimental System and Methodology

The colloidal system selected for this study was polystyrene latex spheres suspended in water. This system was chosen because hard-sphere colloidal suspensions are easily prepared by the addition of NaCl (see below). A hard-sphere suspension corresponds to a system where the potential of interaction of the suspended particles is zero except at particle/particle contact where the interaction potential becomes infinite (Russel et al., 1989). The latex suspensions were acquired from Interfacial Dynamics Corporation (IDC) and the latex particle properties are outlined in Table 2. When necessary, the solutions, as received, were diluted with ultrapure water (NANOpure water system, 18.3 MΩ·cm) or with NaCl solutions to yield the desired weight fraction and NaCl molarity. Suspension weight fraction was determined gravimetrically.

Woods and Krieger (1970) and Krieger (1972) have demonstrated that suspensions of the type used in this study will behave like a hard-sphere suspension if the ionic strength is sufficiently high to provide screening of interparticle Coulombic forces but not too high to promote van der Waals forces. The necessary NaCl molarity required to achieve this effect was determined by measuring the suspension viscosity as a function of NaCl molarity ($0 \le [\text{NaCl}] \le 0.1$). The addition of NaCl to a latex suspension with $\omega_o = 0.9571$ reduced its viscosity, and for salt concentrations in the range $0.04 \le [\text{NaCl}] \le 0.1$ the viscosity was found to be essentially constant and minimized, suggesting that both Coulombic and van der Waals interactions were absent. Our hard-sphere ex-

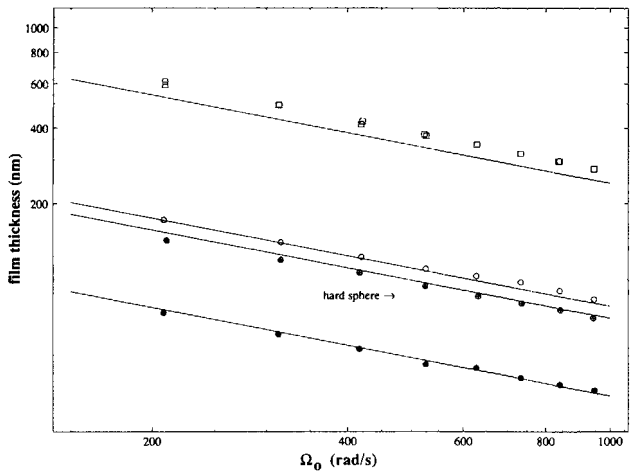

Figure 1. Coated film thickness vs. final substrate angular velocity: comparison of experiment and theory.

Solid lines correspond to the theoretical prediction. Symbols correspond to the experimental results. (⊕) hard-sphere. $\omega_o = 0.9571 \pm 0.0004$, $b = 0.464$; (□) nonhard-sphere, $\omega_o = 0.9147 \pm 0.0007$, $b = 0.517$; (○) nonhard-sphere, $\omega_o = 0.9586 \pm 0.0005$, $b = 0.466$; (●) nonhard-sphere, $\omega_o = 0.9798 \pm 0.0009$, $b = 0.468$.

periment ($\omega_o = 0.9571$) was conducted with [NaCl] = 0.1 to insure that all Coulombic interactions were absent. Since the viscosity and diffusivity constitutive relations for hard-sphere suspensions are known (see Eqs. 15 and 16), no additional physical property measurements were required for the hard-sphere experiment.

We prepared our nonhard-sphere suspensions by simply diluting the latex suspensions obtained from IDC with ultrapure water to yield the desired weight fraction. The suspension viscosity of the nonhard-sphere system was measured as a function of ϕ and the data fitted to Eq. 15 with $\phi_m = 0.183$. As will be explained subsequently, the concentration dependence of the diffusivity for a nonhard-sphere suspension was not required. All viscosity measurements were made with a capillary viscometer.

The solutions were spin-coated onto 4-in. (102-mm) silicon wafers using an EC101 Headway Research, Inc. spin coater. The spin-coating protocol consisted of applying 1 or 2 mL of coating solution to a stationary wafer that was subsequently accelerated to the angular velocity of interest. The acceleration rate of the spin coater was approximately 10^4 rpm/s.

Film thickness and film index of refraction were determined by ellipsometry using a Rudolph AutoE1 II ellipsometer. To eliminate the uncertainty in the film thickness determination, each measurement was taken at three wavelengths: 405, 632.8 and 800 nm.

Results and Discussion

Model validation

In this section, we validate our model by comparing the predicted film thickness with experimental results. Figure 1 shows both the theoretical and experimental coated-film thickness as a function of the angular velocity. One experiment ($\omega_o = 0.9147$) was repeated, and the reproducibility of the measurements was found to be better than 3.3% over the entire angular velocity range. Four sets of experimental data are plotted in Figure 1. One set corresponds to a hard-sphere system, while the remaining three correspond to a nonhard-sphere system with $\phi_m = 0.183$. Overall, the agreement between theory and experiment is excellent for both hard-sphere and nonhard-sphere systems except at high suspension concentrations ($\omega_o < 0.94$). For $\omega_o > 0.94$, the maximum difference between theory and experiment is less than 7.5% for both systems. It should be emphasized that there are no adjustable parameters in the model. The solvent properties used in the model were taken from Table 1, and the suspension viscosity and diffusivity were determined with Eqs. 15 and 16. Values for the dimensionless groups used in the calculations of Figure 1 are shown in Table 3. For weight fractions $\omega_o < 0.94$, the agreement is less satisfactory because of the inaccuracy in the constitutive relation used for the viscosity. In our laboratory, we were not able to make reliable measurements of the viscosity for $\omega_o < 0.9147$, and thus the predictions at high solids concentration are based on an extrapolation of the viscosity measurements, which we believe underpredicts the viscosity at high solids concentration.

The present calculations show that the coated film thickness varies with the angular velocity according to:

$$h_f \propto \Omega_o^{-b} \tag{24}$$

with $b = 0.5$. This dependence has been experimentally observed by Meyerhofer (1978), Lai (1979), Daughton and Givens (1982), Chen (1983), and Bornside et al. (1991), and predicted theoretically by Bornside et al. (1989, 1991), Lawrence (1988, 1990), Meyerhofer (1978), and Ohara et al. (1989). A least squares fit of Eq. 24 to the data in Figure 1 yields b values in the range $0.464 \le b \le 0.517$. Other investigators have observed circumstances where the exponent $b \neq 0.5$ (Meyerhofer, 1978; Skrobis et al., 1990; Lawrence and Zhou, 1991). For example, Lawrence and Zhou (1991) show that shear thinning fluids with a power law behavior will have an exponent $b > 0.5$. Since the measured values of b in our experiments cluster around 0.5 (within experimental error), our assumption that shear thinning effects are unimportant appears reasonable.

The uniformity of the coated film was checked by measuring the film thickness at various radial positions ($0 \le r < 2.5$ cm), and the variation in film thickness was found to be small. Specifically, for the hard-sphere system, the variation was less than 0.3% at 1,930 rpm and less than 1.3% at 8,900 rpm. Note, that with our ellipsometer, we were unable to do a complete radial scan in film thickness to quantify the edge effects.

Fundamentals of spin coating colloidal suspensions

Now that we have validated our model, it is worthwhile examining in some detail the dynamics of film thinning. Our goal is to understand the complex, coupled momentum, mass and energy transport phenomena that govern the process. The base case that we will use for discussion is a colloidal suspension of hard spheres in *ethanol*. The spin coating conditions are 5,000 rpm, impulsive substrate acceleration, $\omega_o = 0.97$, $\omega_\infty = 0.0$, $h_o = 0.5$ mm, $T_o = 298.15$ K, and $T_\infty = 298.15$ K.

For these conditions, the Reynolds number $Re = 121.4$, indicating that inertial effects are important during the initial

Table 3. Calculation Parameters for Specified Substrate Rotation Rate

	Figure 1				Base Cases	
Type	Hard-Sphere	Nonhard-Sphere	Nonhard-Sphere	Nonhard-Sphere	Hard-Sphere	Nonhard-Sphere
ω_o	0.9571	0.9147	0.9586	0.9798	0.97	0.97
T_o (K)	299.82	301.48	301.62	301.62	298.15	298.15
ω_∞	7.22×10^{-3}	8.89×10^{-3}	9.03×10^{-3}	9.03×10^{-3}	0.0	0.0
T_∞ (K)	299.82	301.48	301.62	301.62	298.15	298.15
Ω_o (rpm)	1,930	2,000	1,990	1,990	5,000	5,000
h_o (mm)	0.25	0.123	0.123	0.123	0.5	0.5
solvent	water	water	water	water	ethanol	ethanol
[NaCl] (mol/L)	0.1	0.0	0.0	0.0	—	—
ϕ_m	0.63	0.183	0.183	0.183	0.63	0.15
Re	0.133	1.076	2.345	3.160	121.41	94.21
Sc	28,886.3	77,205.8	40,740.1	32,771.8	44,668.9	57,564.6
Pr	6.654	21.364	9.774	7.264	16.56	21.34
Bi	22,440.9	94,915.8	109,456.1	118,597.3	651,278.2	651,278.2
Bi_h	1.138×10^{-3}	5.793×10^{-3}	5.778×10^{-3}	5.778×10^{-3}	0.1352	0.1352
N	1.35	1.35	1.35	1.35	2.204	2.204
ϵ	0.317	0.308	0.289	0.321	—	—

Note that $Re\propto\Omega_o$ and Bi, $Bi_h\propto\Omega_o^{1/2}$.

stages of film thinning (values for the other dimensionless groups are listed in Table 3). Figure 2 shows the instantaneous film thickness as a function of spinning time for our base case and for the case when the inertial terms other than centrifugal in Eqs. 3b-3c are neglected. The latter approximation to the hydrodynamics is identical to that used by Bornside et al. (1989, 1991), Lawrence (1988, 1990), and Meyerhofer (1978) to study spin coating of viscous solutions ($Re\ll 1$). When inertia is included and $Re\gg 1$, the thinning rate is initially reduced because the development of a hydrodynamic boundary layer at the disk surface prevents the angular velocity of the substrate from being imparted to the film instantaneously (Higgins, 1986; Rehg and Higgins, 1988). However, after 16 rad, approximately 30 ms, the thinning rates predicted from the two models are comparable.

A more detailed view of the thinning dynamics is shown in Figure 3. We discuss first the convective and evaporative thinning rates, $\dot{C}$ and $\dot{E}$. Film inertia and boundary layer growth cause both these rates to increase from the onset of spinning until approximately 10 rad. Since the centrifugal force field increases with the square of the angular velocity, the convective thinning rate continually increases during film spin-up. After 10 rad, however, the film has thinned considerably as shown by the film thickness profile (see also Figure 2), and viscous forces become significant causing the convective thinning rate to pass through a maximum before decreasing, first slowly and then precipitously. Interestingly, during the period of decreasing $\dot{C}$, the cumulative evaporative loss $I\dot{E}$ is of the same order of magnitude as the cumulative convective loss $I\dot{C}$, although this is not evident in the plot. Figure 4 confirms that the solvent concentration in the film does not decrease significantly from its initial value until well into the spinning time: $\tau > 100$ rad. Thus, the viscous forces that inhibit film thinning are primarily a consequence of the thinness of the film and secondarily a consequence of the enhanced viscosity due to solvent loss.

Since the mass-transfer coefficient is proportional to the

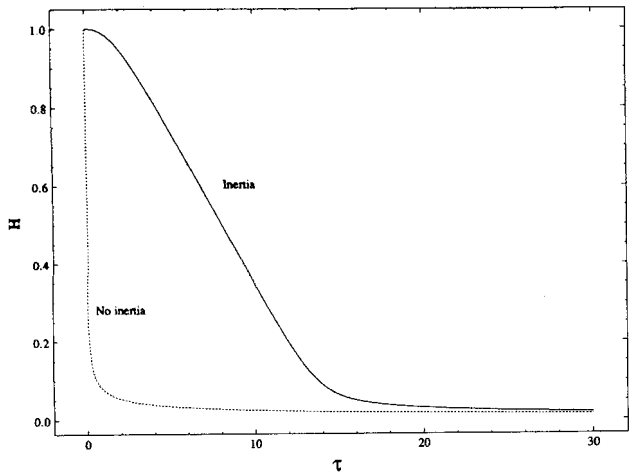

Figure 2. Dynamic film thickness vs. spinning time: effect of inertia on film thinning.

Spin-coating parameters: 5,000 rpm, impulsive acceleration, $\omega_o=0.97$, $\omega_\infty=0.0$, $h_o=0.5$ mm, $T_o=298.15$ K, $T_\infty=298.15$ K, $\phi_m=0.63$.

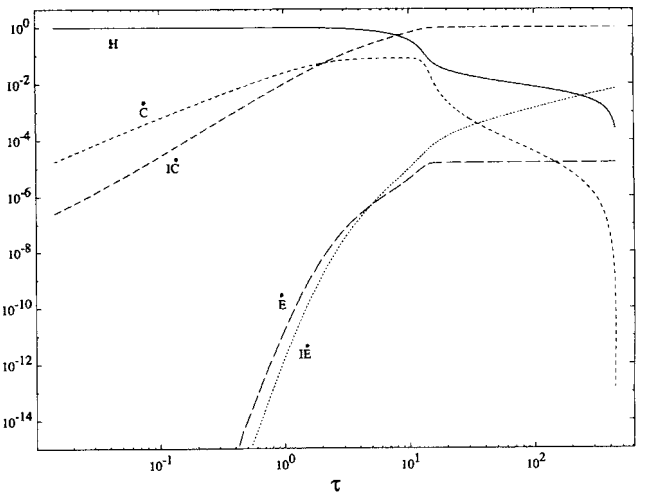

Figure 3. Film thinning dynamics as a function of spinning time.

Parameters are the same as those in Figure 2.

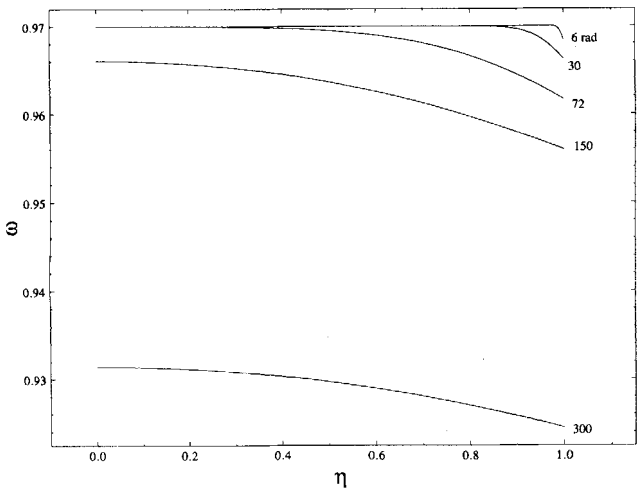

Figure 4. Solvent weight fraction profiles in the thinning film for various values of the spinning time.

Parameters are the same as those in Figure 2.

square root of the free surface angular velocity, there is also an increase in the evaporation rate at short times during film spin-up. Once the angular velocity of the film is equal to that of the substrate, the evaporation rate attains a *constant value*. The reason for this is that the evaporation rate is dictated by the gas-phase mass-transfer resistance, which is constant except during film spin-up (since $\bar{\omega}$ is insensitive to the film-side concentration of solvent as mentioned earlier). Consequently, our predictions for the nonhard-sphere colloidal suspensions are successful (cf. Figure 1), even though the constitutive relation used for the diffusivity is strictly valid only for hard-sphere suspensions. An improved constitutive relation will not alter the predicted film thickness (since the evaporation rate is constant), but it will modify the concentration profiles from those shown in Figure 4. It is unclear whether this result will hold for systems that are not colloidal such as in polymer systems. In polymer systems, the diffusivity decreases with decreasing solvent concentration and the film-side mass-transfer resistance increases, possibly becoming greater than the gas-side mass-transfer resistance and thus modifying the evaporation rate (cf. Bornside et al., 1989). The same effect does not occur in our system because the diffusivity *increases* (see Eq. 16) as the solvent concentration decreases, and thus there is always an attendant decrease in the film-side mass-transfer resistance. In conjunction with the thinness of the film and the large Schmidt number (see Table 3), this results in a negligible film-side mass-transfer resistance as indicated by the small concentration gradients in Figure 4.

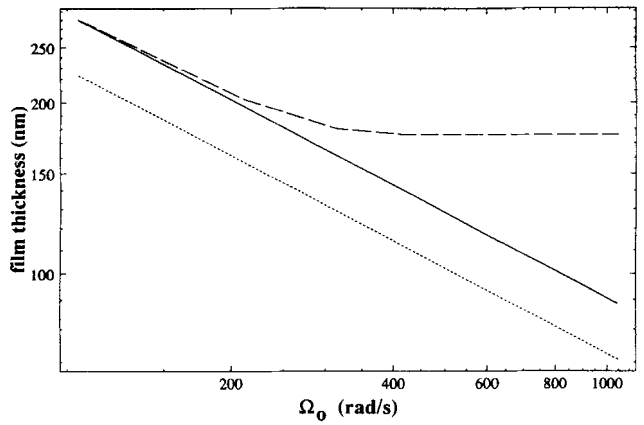

Figure 5. Theoretically predicted coated film thickness vs. final substrate angular velocity.

Effect of substrate acceleration: (——) impulsive acceleration; (— — —) constant acceleration of 209.44 rad/s^2; (- - - - -) impulsive acceleration, Eq. 1a. All other parameters are the same as those in Figure 2.

It has been observed that under certain circumstances the film thickness does not behave according to Eq. 24 regardless of the value of b (see, for example, Rehg et al., 1989). We show that the acceleration rate of the spin coater can be a factor, since it does modify the inverse power law dependence on angular velocity. This effect is expected to be important in spin-coating large area substrates where the inertia of the disk prevents instantaneous (or more practically, rapid) acceleration of the substrate.

Figure 5 shows the film thickness vs. the angular velocity of the substrate for two substrate acceleration protocols, instantaneous acceleration, and a finite acceleration of 2,000 rpm/s. When the acceleration rate is finite, the film thickness is no longer proportional to $\Omega_o^{-1/2}$ at high angular velocities. Specifically, the film thickness becomes independent of Ω_o, because the coated film reaches its final thickness while the substrate is still accelerating. At low rotation rates the effect of different acceleration protocols is negligible, since the time required for radial outflow to cease exceeds the time required for the substrate to reach its final angular velocity.

Also plotted in Figure 5 is the prediction from Eq. 1a for impulsive acceleration (substrate inertia during spin-up cannot be addressed with this model). The model underpredicts the computed film thickness by nearly 70 nm for the angular velocity range studied. There are several reasons for this. First, Eq. 1a is derived by assuming that radial outflow ceases when the convective thinning rate (in the absence of evaporation) equals the evaporative thinning rate. For the coating parameters used, a simple calculation based on the derivation of Eq. 1a predicts that these two thinning rates are equal when $\tau = 182$ rad, whereas Figure 5 shows that, in fact, $\dot{C} = \dot{E}$ when $\tau = 148$ rad. Consequently, Eq. 1a overpredicts the cumulative convective losses $I\dot{C}$ and hence underpredicts the film thickness. These losses can be significant if the coated film is very thin (the case of interest), since it is the cumulative convective loss that is important. Second, during the initial phase of thinning, Eq. 1a does not account for the increase in the suspension viscosity associated with solvent evaporation. While this has a minor effect on the convective thinning rate for hard-sphere suspensions, it is significant for systems where the viscosity is much more sensitive to the concentration, for example, non-hard-sphere suspensions and concentrated polymer solutions. The experiments of Bornside et al. demonstrates this shortcoming where poor agreement between theory and experiment at high polymer concentrations was observed.

The theory developed by Lawrence (1988, 1990), Eq. 1b, is based on the simplifying assumption that convective thinning ceases when the concentration boundary layer reaches the substrate. This approximation appears overly restrictive for the spin coating of colloidal suspensions. Our calculations show that even after the concentration boundary layer reaches the

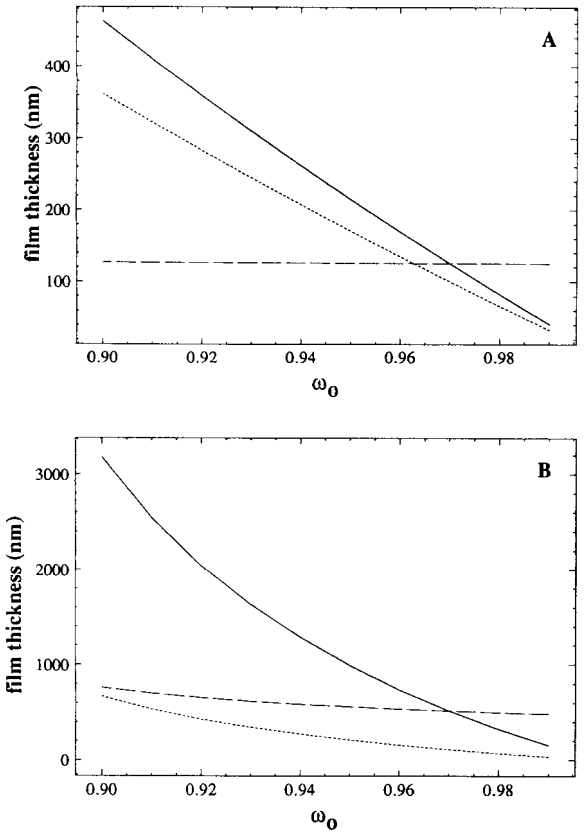

Figure 6. Theoretically predicted coated film thickness vs. initial solvent weight fraction.

(——) this study; (-----) Eq. 1a; (———) Eq. 1b. (A) $\phi_m = 0.63$, $C = 0.04133$; (B) $\phi_m = 0.15$, $C = 0.1605$. All other parameters are the same as those in Figure 2.

substrate ($\tau = 72$ rad), the convective loss rate, though small, is not negligible and contributes to an *additional* 1.975 μm of thinning. Consequently, the parameter C in Eq. 1b that must be chosen to bring Lawrence's (1988) theory into agreement with our results is not $Q(1)$ as he suggests, but several orders of magnitude smaller: $C = 0.041$.

Since the predicted film thickness is not sensitive to the constitutive relation used for $\mathfrak{D}$, it is of interest to examine nonhard-sphere systems by simply changing ϕ_m in Eq. 15. In Figure 6, we explore the effect of changing ϕ_m by plotting the film thickness as a function of the initial solvent weight fraction for representative values of ϕ_m. When $\phi_m = 0.63$ (Figure 6a, the hard-sphere case), the final thickness is very nearly linear in the initial solvent weight fraction. The functional dependence becomes nonlinear when $\phi_m = 0.15$ (Figure 6b), indicating that the viscosity of the coating solution is greater and more sensitive to changes in the film solvent concentration. This suggests that the dependence of the coated film thickness on initial concentration is system-dependent, and a simple correlation between coated film thickness and initial concentration probably does not exist. Figures 6a and 6b make this clear where we show the predictions of Eqs. 1a and 1b. Not only do both equations have the incorrect functional dependence on ω_o, they also underpredict the theory developed here (note that the parameter C in Eq. 1b is chosen so that there is coincidence with our results at $\omega_0 = 0.97$).

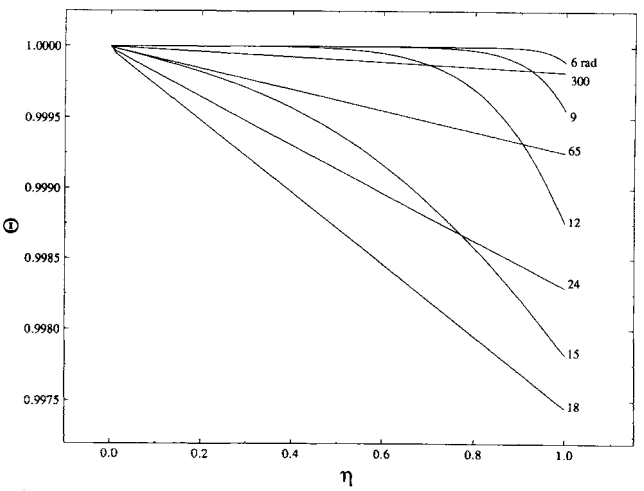

Figure 7. Temperature profiles in the thinning film for various values of spinning time.

Parameters are the same as those in Figure 2.

The latent heat of vaporization induces evaporative cooling at the free surface. The film temperature profiles that result from evaporative cooling are shown in Figure 7. During the initial stages of spin-up, the energy flux is directed into the film from the constant temperature substrate and from the overlying gas phase. After 12 rad, the temperature boundary layer approaches the substrate, and shortly thereafter ($\tau = 18$ rad) the free surface temperature reaches it minimum value, before increasing. Energy transport in the film is then quasi-steady, resulting in the linear temperature profiles shown in Figure 7. The implications of the temperature drop across the film are discussed in the next section.

Influence of spinning protocols on striations

It is well known that under certain spin-coating conditions it is not possible to coat a film of uniform thickness. The coating may instead exhibit radial striations with variable amplitude (Rehg and Higgins, 1992; Frasch and Saramski, 1982)

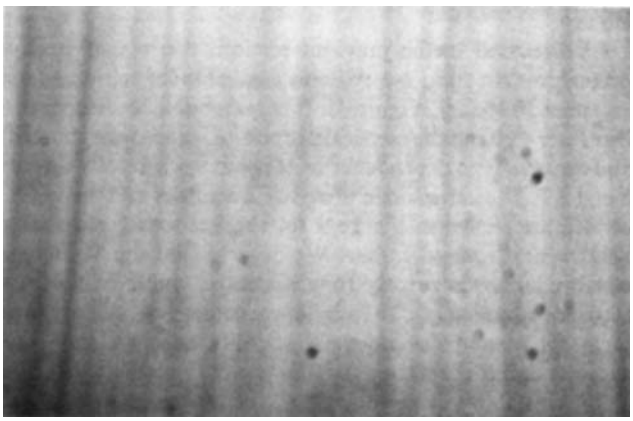

Figure 8. Example of radial striations observed in spin coating a SiO_2 colloidal suspension.

Magnification: 50x. The spots are dust particles on the microscope optics.

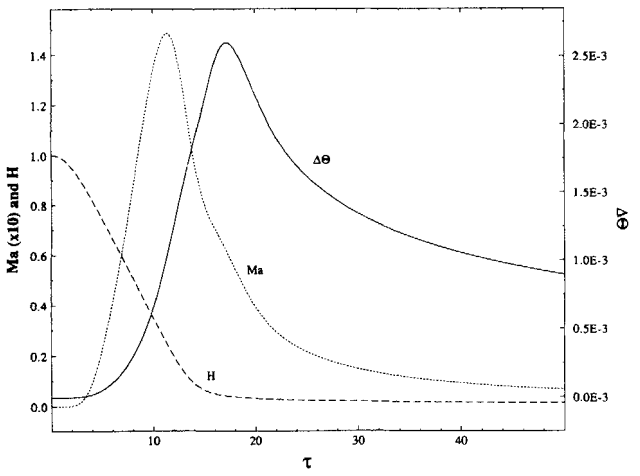

Figure 9. Instantaneous Marangoni number, film thickness, and temperature drop across the film vs. spinning time.

Parameters are the same as those in Figure 2.

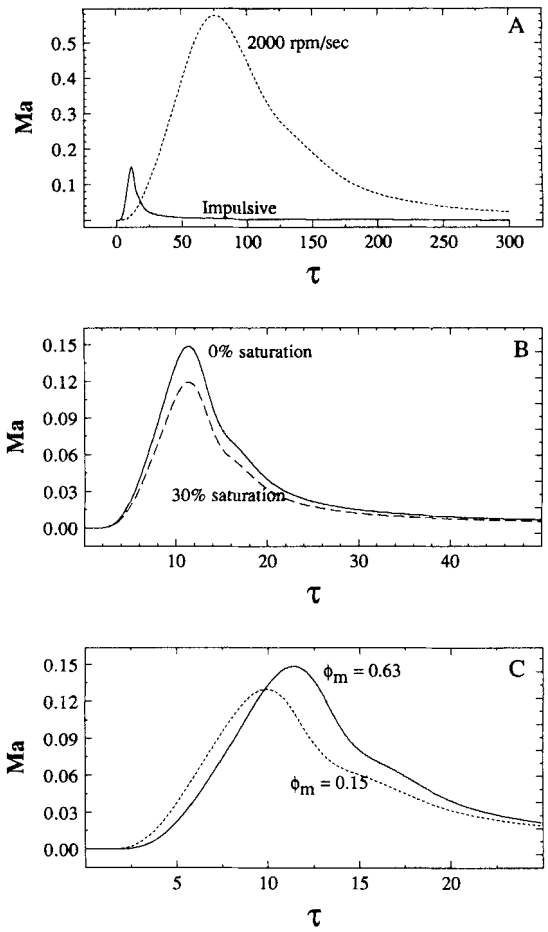

Figure 10. Effect of spin-coating protocol on the instantaneous Marangoni number.

(A) Effect of substrate acceleration.

(B) Effect of partially saturating the overlying gas phase with solvent.

(C) Effect of initial viscosity.

Except where noted the parameters are the same as those in Figure 2.

as illustrated in Figure 8. The photograph shows a SiO_2 colloidal coating spin-coated at 2,000 rpm, with an acceleration rate of approximately 1,000 rpm/s. The SiO_2 colloidal suspension was prepared by the Stöber process with ethanol as the solvent, and the nominal particle diameter was 20 nm. The coated film is obviously nonuniform and marked with radial striations. These striations are believed to be caused by evaporative convection, and in another study we have argued that the dominant driving force for this instability is surface tension gradients: the Marangoni effect (Rehg and Higgins, 1992).

A qualitative understanding of how this instability arises in the spin coating of colloidal suspensions can be ascertained by examining how different spin-coating protocols influence the instantaneous Marangoni number defined as:

$$Ma = \left(\frac{\partial \sigma}{\partial T}\right)\frac{\Delta T h}{\mu \alpha} \tag{25}$$

where σ is the surface tension of the fluid, and ΔT is the temperature drop across the film induced by evaporative cooling. Other variables appearing in Eq. 25 are as defined previously.

As discussed in the previous section, the weight fraction drop across the film, $\Delta\omega$, remains negligible for spinning times less than 30 rad (cf. Figure 4). It is reasonable to assume then that for $\tau < 30$ rad the physical properties μ and α are constant, and thus the time dependence in *Ma* enters principally through h and ΔT. The variation in these two quantities and their effect on *Ma* are shown in Figure 9 for the base-case spin-coating conditions discussed earlier. We observe that the Marangoni number increases rapidly to a maximum value in the early stages of spinning ($\tau < 20$ rad) before decreasing. Although we have not carried out a formal stability analysis, this result suggests that if the stationary film ($\tau < 0$) is unstable to a Marangoni instability (Pearson, 1958), then spinning the disk will tend initially to enhance the instability because of the increased evaporation rate, before the stabilizing effects of increasing viscosity and decreasing film thickness intervene.

Frasch and Saremski (1982) have shown that the substrate acceleration rate has a strong influence on film stability, and we begin our discussion by quantifying this effect in terms of *Ma*. In Figure 10a, we plot the predicted Marangoni number vs. spinning time for our base case under impulsive acceleration and finite acceleration (2,000 rpm/s). Not only is *Ma* larger for the ramped case, but it remains significant for a longer spinning time. The reason for this is that the film does not thin as rapidly when the substrate is ramped. Any protocol that enhances the thinning is expected to reduce *Ma*. For example, our calculations show that increasing the spinning speed decreases *Ma*, and our experiments show that the same protocol suppresses striation formation in the film (Rehg and Higgins, 1992).

Elliott and Hockey (1979) have indicated that partial saturation of the overlying gas phase with coating solution solvent is also an effective means of reducing the amplitude of the striations. The calculations support this view as seen in Figure 10b where we plot the Marangoni number vs. spinning time for a solvent-free overlying gas phase and for an overlying gas

Table 4. Effect of NaCl Molarity on Film Porosity (ϵ) and the Spin Parameter (b)

NaCl Molarity	Film Porosity, ϵ	Spin Parameter, b
0.0	0.33	0.51
0.004	0.35	0.49
0.007	0.35	0.47
0.01	0.36	0.5
0.04	0.45	0.47
0.07	0.47	0.45
0.1	0.49	0.44
cml	—	0.43
SiO_2/Chlorobenzene	—	0.38
SiO_2/Toluene	—	0.30

phase that is 30% saturated with solvent. When the overlying gas phase is partially saturated, the driving force for mass transfer is reduced, resulting in a reduced evaporative cooling rate. The net result is that the temperature drop across the film and *Ma* are lower. A lower evaporation rate does increase the time required for radial outflow to cease, resulting in a thinner coated film ($\sim 7\%$).

We now examine how the initial viscosity of the suspension influences *Ma*. Figure 10c shows *Ma* plotted against spinning time for our base case when $\phi_m = 0.63$ and $\phi_m = 0.15$. Increasing the initial viscosity reduces *Ma*, even though the film thins more slowly. Thus, it appears possible to use this strategy in conjunction with higher rotation rates to produce striation-free films with the desired thickness. This strategy is examined in another publication (Rehg and Higgins, 1992) where we report experimental results for polymer solutions that show striation-free coatings at high initial concentrations.

Finally, it is worth noting that a judicious choice of solvent will greatly reduce the magnitude of *Ma*. For example, the maximum *Ma* in Figure 9 is 0.148. If we repeat this calculation with the same spinning parameters except with water rather than ethanol as the solvent, then the maximum *Ma* is 0.014. Indeed, we have never observed striations in any of the water-based systems used here, while we have seen striations in ethanol-based systems (cf. Figure 8).

Concluding Remarks

We have presented a reasonably complete analysis of the physics that govern spin coating of colloidal suspensions, obtained by numerically solving the self-similar form of the Navier-Stokes, convective diffusion and thermal energy equations. Self-similarity arises due to the imposed constraint that the film-free surface remains flat (Higgins, 1986). The model, absent of any adjustable parameters, is shown to be in excellent agreement with experiments conducted with both hard-sphere and nonhard-sphere colloidal suspensions of latex spheres and shows promise as a predictive spin-coating model for more general applications, once the constitutive relations for the coating solution viscosity and solvent diffusivity are known.

The theoretical results highlight several important differences between the spin coating of colloidal and polymeric suspensions. First, the functional relationship between the viscosity and concentration in the coating solution appears to play a much more significant role in spin coating of colloidal suspensions than in polymeric suspensions. This is especially true in nonhard-sphere colloidal suspensions where small changes in concentration can yield large changes in the suspension viscosity. Second, the results show that the timescales associated with spin coating of colloidal suspensions are rather disparate from those associated with the spin coating of polymeric suspensions, and thus the simple approximations, used by Bornside et al. (1991), Meyerhofer (1978), and Lawrence (1988, 1990) for predicting coated-film thickness in polymeric systems, are inadequate for evaluating the spin coating of colloidal suspensions.

In nonhard-sphere colloidal suspensions, there are a variety of physical effects that cannot be addressed by the present model. For example, it is well known that coated-film structure can exhibit extraordinary order (Deckman and Dunsmuir, 1982). To account for structure effects, it is necessary to include in the model the forces by which colloidal particles interact (for example, van der Waals and Coulombic forces). During the coating process, these forces will be modified by local changes in concentration, temperature, and pH, all of which influence the coating solution viscosity (ϕ_m) and the diffusivity. Ultimately, these forces will dictate the film porosity. We have been able to demonstrate some of these effects experimentally by examining the porosity of the coated film as a function of initial [NaCl]. The results are shown in Table 4. In these experiments, we spin-coated latex suspensions of approximately the same weight fraction, but with different [NaCl]. The porosity of the coated films was observed to increase monotonically with [NaCl].

Our experiments suggest that colloidal interactions may also determine the functional relationship between the coated film thickness and substrate angular velocity: the exponent b in Eq. 24. The overall trend observed was that the exponent b decreased with increasing [NaCl] (Table 4). Limited experiments were conducted with 21-nm-dia. carboxylate modified polystyrene latex spheres suspended in water (IDC, Lot No. 10-216-5), termed "fuzzy" particles because of their porous surface layer of carboxylate groups, and 20-nm-dia. SiO_2 particles sterically stabilized with stearyl groups suspended in toluene and chlorobenzene (prepared according to the method of Van Helden et al., 1981). Both of these experiments yielded rather low values of b (Table 4). At this time, we have no rational explanation for these effects and further experiments are needed to fully understand the colloidal effects in these systems.

The local charge distribution on the substrate may influence film structure and film thinning. For example, a substrate and colloidal dispersion of like charge could give rise to a depletion layer of lower viscosity adjacent to the substrate that in principle would allow one to coat thinner films. Depletion layer effects have already been observed in foams (Kruglyakov and Meshkova, 1990) and polymer systems (Müller-Mohnssen et al., 1990), but to our knowledge have not been studied in spin coating.

Finally, we have used our model to examine a possible mechanism for a secondary Marangoni instability during spin coating. Protocols for spin-coating, striation-free coatings were evaluated with the model and shown to be in accordance with the limited experimental data available. In particular, protocols that entail fast substrate acceleration, high spinning speeds, and reduced evaporation rates were acknowledged as most likely to result in uniform coatings. Other alternatives are possible and may be identified through a formal analysis of the Marangoni instability in spin coating. The model presented

in this article provides a base flow for such a stability analysis. We hope to report on the outcome of such an analysis at a future time.

Acknowledgment

The authors are grateful to the San Diego Supercomputer Center for providing supercomputer time and to Dr. Albert P. Philipse of the Van't Hoff Laboratory, University of Utrecht for supplying the SiO_2 particles prepared by the method of Van Helden et al. (1981).

This work was supported in part by Lawrence Livermore National Laboratory, Tektronix, Inc., and the California Space Institute.

Notation

a = particle radius, m
$\underline{A}$ = coefficient matrix of finite difference form of Eq. 3c
b = spin parameter
$\underline{B}$ = coefficient matrix of finite difference form of Eq. 3b
Bi, Bi_h = Biot number for mass and heat transfer
C_p = constant pressure heat capacity, J/(kg·K)
$\underline{D}$ = load matrix of finite difference form of Eq. 3c
$\mathfrak{D}$, $\tilde{\mathfrak{D}}$, $\mathfrak{D}_g$, $\mathfrak{D}_o$ = Gradient diffusivity, Stokes-Einstein diffusivity, solvent diffusivity in the gas phase, initial diffusivity, m^2/s
$\overline{\mathfrak{D}}$ = diffusivity functional, $\mathfrak{D}/\mathfrak{D}_o$
$\underline{E}$ = load matrix of finite difference form of Eq. 3b
$\mathbf{e}_r$, $\mathbf{e}_z$, $\mathbf{e}_\theta$ = basis vectors in radial, axial, and angular directions
f = radial velocity function, s^{-1}
F = dimensionless radial velocity function
g = angular velocity function, s^{-1}
G = dimensionless angular velocity function
h, h_f, h_o = instantaneous, coated, and initial film thickness, m
H = dimensionless film thickness
ΔH_{vap} = enthalpy of vaporization, J/kg
k_b = Boltzman constant
k_m, k_h = mass- and heat-transfer coefficients, m/s and W/(m^2·K)
k_g, k_o, k_s = gas phase, initial, and solvent thermal conductivities, W/(m·K)
Ma = Marangoni number
M_s = solvent molecular weight
M_g = air molecular weight
N = dimensionless enthalpy of vaporization
n_d, n_p = indexes of refraction of dense and porous films
Pr, Pr_g = film and gas phase Prandtl numbers
P_s^{vap} = solvent vapor pressure, atm
P_{tot} = ambient pressure, taken to be 1 atm
r = distance in radial direction, cylindrical system, m
Re = Reynolds number
Sc, Sc_g = film and gas phase Schmidt numbers
t = time, s
T, T_o = instantaneous and initial temperatures, K
ΔT = temperature drop across the film, K
$\mathbf{u}$ = velocity vector, m/s
w = axial velocity, m/s
W = dimensionless axial velocity
y_s = gas phase mole fraction solvent at free surface
z = distance in axial direction, cylindrical system, m

Greek letters

α_o, α_s = initial and solvent thermal conductivities, m^2/s
β = grid transformation parameter
δ = relative error
ϵ = coated film porosity
ϕ = volume fraction suspended material
ϕ_m = volume fraction suspended material when suspension viscosity is unbounded
γ = molecular weight ratio of solvent to air, M_s/M_g
η = dimensionless axial coordinate
λ = wavelength at which index of refraction is measured, m
μ, μ_s = suspension and solvent viscosity, Pa·s
ν, ν_g, ν_o, ν_s = suspension, gas phase, initial, and solvent kinematic viscosities, m^2/s
$\bar{\nu}$ = kinematic viscosity functional, ν/ν_o
θ = angular coordinate in cylindrical system
Θ, Θ_∞ = dimensionless temperature in the film and in the gas phase far from the free surface
ρ, $\bar{\rho}$, ρ_s = suspension, gas phase, and solvent density, kg/m^3
σ = surface tension, N/m
τ = dimensionless time
ω, ω_o = instantaneous and initial weight fraction solvent
$\bar{\omega}$, ω_∞ = weight fraction solvent in gas phase at the free surface and far from the free surface
Ω, Ω_o = instantaneous and terminal substrate rotation rate, rpm or rad/s
Ω_i = free surface angular velocity, rpm or rad/s
ξ = computation domain axial coordinate

Literature Cited

Batchelor, G. K., "Brownian Diffusion of Particles with Hydrodynamic Interaction," *J. Fluid Mech.*, **74**, 1 (1976).

Benton, E. R., "On the Flow Due to a Rotating Disk," *J. Fluid Mech.*, **24**, 781 (1966).

Bornside, D. L., C. W. Macosko, and L. E. Scriven, "Spin Coating: One-Dimensional Model," *J. Appl. Phys.*, **66**, 5185 (1989).

Bornside, D. L., C. W. Macosko, and L. E. Scriven, "Spin Coating of a PMMA/Chlorobenzene Solution," *J. Electrochem. Soc.*, **138**, 317 (1991).

Buscall, R., J. W. Goodwin, M. W. Hawkins, and R. H. Ottewill, "Viscoelastic Properties of Concentrated Lattices," *J. Chem. Soc., Farad. Trans. 1*, **78**, 2873 (1982).

Chen, B. T., "Investigation of the Solvent-Evaporation Effect on Spin Coating of Thin Films," *Polym. Eng. Sci.*, **23**, 399 (1983).

Daughton, W. J., and F. L. Givens, "An Investigation of the Thickness Variation of Spun-on Thin Films Commonly Associated with the Semiconductor Industry," *J. Electrochem. Soc.*, **129**, 173 (1982).

de Kruif, C. G., E. M. F. van Iersel, and A. Vrij, "Hard Sphere Colloidal Dispersions: Viscosity as a Function of Shear Rate and Volume Fraction," *J. Chem. Phys.*, **83**, 4717 (1985).

de Kruif, C. G., J. W. Jansen, and A. Vrij, "Sterically Stabilized Silica Colloid as a Model Supramolecular Fluid," *Physics of Complex and Supermolecular Fluids*, S. A. Safran and N. A. Clark, eds., Wiley-Interscience (1987).

Deckman, H. W., and J. H. Dunsmuir, "Natural Lithography," *Appl. Phys. Lett.*, **41**, 377 (1982).

Elliott, D. J., and M. A. Hockey, "One Micron Range Photoresist Imaging: a Practical Approach," *Solid State Technol.*, **22**, 53 (1979).

Emslie, A. G., F. T. Bonner, and L. G. Peck, "Flow of a Viscous Liquid on a Rotating Disk," *J. Appl. Phys.*, **29**, 858 (1958).

Frasch, P., and K. H. Saremski, "Feature Size Control in IC Manufacturing," *IBM J. Res. Dev.*, **26**, 561 (1982).

Higgins, B. G., "Film Flow on a Rotating Disk," *Phys. Fluids*, **29**, 3522 (1986).

Homsy, G. M., and J. L. Hudson, "Transient Flow Near a Rotating Disk," *Appl. Sci. Res.*, **18**, 384 (1968).

Kreith, F., J. H. Taylor, and J. P. Chong, "Heat and Mass Transfer from a Rotating Disk," *J. Heat Trans.*, **81**, 95 (1959).

Krieger, I. M., "Rheology of Monodisperse Lattices," *Adv. Colloid Interf. Sci.*, **3**, 111 (1972).

Kruglyakov, P. M., and T. V. Meshkova, "Flow of Foams in the Slip Regime," *Kolloidnyi Zhurnal*, **52**, 487 (1990).

Lai, J. H., "An Investigation of Spin Coating of Electron Resists," *Polym. Eng. Sci.*, **19**, 1117 (1979).

Lawrence, C. J., "The Mechanics of Spin Coating of Polymer Films," *Phys. Fluids*, **31**, 2786 (1988).

Lawrence, C. J., "Spin Coating with Slow Evaporation," *Phys. Fluids A*, **2**, 453 (1990).

Lawrence, C. J., and W. Zhou, "Spin Coating of Non-Newtonian Fluids," *J. Non-Newt. Fluid Mech.*, **39**, 137 (1991).

Meyerhofer, D., "Characteristics of Resist Films Produced by Spinning," *J. Appl. Phys.*, **49**, 3993 (1978).
Müller-Mohnssen, H., D. Weiss, and A. Tippe, "Concentration Dependent Changes of Apparent Slip in Polymer Solution Flow," *J. Rheol.*, **34**, 223 (1990).
Ohara, T., Y. Matsumoto, and H. Ohashi, "The Film Formation Dynamics in Spin Coating," *Phys. Fluids A*, **1**, 1949 (1989).
Pearson, J. R. A., "On Convection Cells Induced by Surface Tension," *J. Fluid Mech.*, **4**, 489 (1958).
Perry, R. H., D. W. Green, and J. O. Maloney, eds., *Perry's Chemical Engineer's Handbook*, McGraw Hill, New York (1984).
Rehg, T. J., and B. G. Higgins, "The Effects of Inertia and Interfacial Shear on Film Flow on a Rotating Disk," *Phys. Fluids*, **31**, 1360 (1988).
Rehg, T. J., J. A. Ochoa-Tapia, A. Knoesen, and B. G. Higgins, "Solgel Derived Tantalum Pentoxide Films as Ultraviolet Antireflective Coatings for Silicon," *Appl. Opt.*, **28**, 5215 (1989).
Rehg, T. J., and B. G. Higgins, "Evaporative Convection in Spin Coating," *AIChE J.*, to be submitted (1992).
Reid, R. C., J. M. Prausnitz, and T. K. Sherwood, *The Properties of Gases and Liquids*, McGraw Hill, New York (1977).
Russel, W. B., D. A. Saville, and W. R. Schowalter, *Colloidal Dispersions*, Cambridge Univ. Press, Cambridge (1989).
Roberts, G. O., "Computational Meshes for Boundary Layer Problems," *Proc. Int. Conf. Num. Methods Fluid Dyn., Lecture Notes in Physics*, Vol. 8, p. 171, Springer-Verlag, New York (1971).
Skrobis, K. J., D. D. Denton, and A. V. Skrobis, "Effect of Early Solvent Evaporation on the Mechanism of Spin-Coating of Polymeric Solutions," *Poly. Eng. Sci.*, **30**, 193 (1990).
Sparrow, E. M., and J. L. Gregg, "Heat Transfer from a Rotating Disk to Fluids of Any Prandtl Number," *J. Heat Trans.*, **81**, 249 (1959).
Swalen, J. D., R. Santo, M. Tacke, and J. Fischer, "Properties of Polymeric Thin Films by Integrated Optical Techniques," *IBM J. Res. Dev.*, **21**, 168 (1977).
Thomas, I. M., "Single Layer Al_2O_3-H_2O and Multilayer Al_2O_3-H_2O-SiO_2 Optical Coatings Prepared from Colloidal Suspensions," *Appl. Opt.*, **28**, 4013 (1989).
Van Helden, A. K., J. W. Jansen, and A. Vrij, "Preparation and Characterization of Spherical Monodisperse Silica Dispersions in Nonaqueous Solvents," *J. Coll. Interf. Sci.*, **81**, 354 (1981).
Weast, R. C., ed., *Handbook of Chemistry and Physics*, CRC Press, Cleveland (1975).
Woods, M. E.,, and I. M. Krieger, "Rheological Studies on Dispersion of Uniform Colloidal Spheres: I. Aqueous Dispersions in Steady Shear Flow," *J. Coll. Interf. Sci.*, **34**, 91 (1970).
Yoldas, B. E., "Investigations of Porous Oxides as an Antireflective Coating for Glass Surfaces," *Appl. Optics*, **19**, 1425 (1980).

Manuscript received Oct. 3, 1991, and revision received Jan. 21, 1992.